Geomechanics and Engineering, *Vol. 23, No. 5 (2020) 467-480*
DOI: https://doi.org/10.12989/gae.2020.23.5.467

Fracture properties and tensile strength of three typical sandstone materials under static and impact loads

Lei Zhou[1,2], Caoyuan Niu[2], Zheming Zhu*[2], Peng Ying[2], Yuqing Dong[2] and Shuai Deng[2]

[1]*Key Laboratory of Deep Earth Science and Engineering (Ministry of Education), College of Architecture and Environment, Sichuan University, Chengdu, 610065, China*
[2]*State Key Laboratory of Hydraulics and Mountain River Engineering, College of Architecture and Environment, Sichuan University, Chengdu, 610065, China*

(Received October 24, 2019, Revised November 16, 2020, Accepted November 27, 2020)

Abstract. The failure behavior and tensile strength of sandstone materials under different strain rates are greatly different, especially under static loads and impact loads. In order to clearly investigate the failure mechanism of sandstone materials under static and impact loads, a series of Brazilian disc samples were used by employing green sandstone, red sandstone and black sandstone to carry out static and impact loading splitting tensile tests, and the failure properties subjected to two different loading conditions were analyzed and discussed. Subsequently, the failure behavior of sandstone materials also were simulated by finite element code. The good agreement between simulation results and experimental results can obtain the following significantly conclusions: (1) The relationship of the tensile strength among sandstone materials is that green sandstone < red sandstone < black sandstone, and the variation of the tensile sensitivity of sandstone materials is that green sandstone > red sandstone > black sandstone; (2) The mainly cause for the difference of dynamic tensile strength of sandstone materials is that the strength of crystal particles in sandstone material, and the tensile strength of sandstone is proportional to the fractal dimension; (3) The dynamic failure behavior of sandstone is greatly different from that of static failure behavior, and the dynamic tensile failure rate in dynamic failure behavior is about 54.92%.

Keywords: sandstone; static loads; impact loads; Brazilian Disc; tensile strength; failure modes

1. Introduction

Rock material is usually considered as brittle materials for investigating related research, its compressive strength is much greater than tensile strength under impact and static loads, and the failure behavior of rock materials under numerous working conditions performs tensile failure characteristics. For the tensile strength of rock materials, it can be divided into two categories: one is static tensile strength, the other is dynamic tensile strength. The static tensile strength is usually obtained indirectly through the static splitting test of the Brazilian Disk (BD) samples by using an electro-hydraulic servo press. The dynamic tensile strength is usually obtained indirectly through the dynamic splitting test of BD sample by using split Hopkinson pressure bar (SHPB) equipment. The two tensile strength calculation approaches have been adopted by a great many of scholars (Bahaaddini *et al.* 2019, Haeri *et al.* 2014, Sarfarazi *et al.* 2017, Wang *et al.* 2018, Wei *et al.* 2016).

When rock materials are subjected to static loads or dynamic loads, its mechanical properties are greatly different in testing process, and the failure behavior perform greatly differences with the variation of loading rates. Especially the basic mechanical parameters of rock materials: when the loading rate increases, the tensile strength and compressive strength of rock will increase significantly. However, there are few investigations on the failure properties of rock materials under dynamic loading through numerical simulation, such as impact loading, especially for different types of sandstone materials under same impact loads. Therefore, this study aims to study the failure behavior of different types of sandstone materials under dynamic and static loads for systematic analysis (Hang *et al.* 2016, Sheikh *et al.* 2019, Wang *et al.* 2019a).

In the aspect of static loads research, many researchers have made significantly achievements on rock materials strength test (Feng *et al.* 2016, Huang *et al.* 2015, Li and Wong 2013, Wu *et al.* 2020, Zhang *et al.* 2018). Yuan and Shen (2017) numerically simulated the stress distribution and failure properties of Brazilian disk by utilizing continuum discrete element code, and analyzed the change of static tensile strength under different contact conditions. Nezhad *et al.* (2018) investigated the effect of different joint inclination angle on the tensile strength of Brazilian disk samples by the stochastic finite element theory, they proposed that the effect of shale heterogeneity on crack evolution must be considered. Yi *et al.* (2018) have carried out static cyclic loading to investigate the variation of tensile strength of Brazilian disk sample under dynamic loading, and then conducted the corresponding numerical simulation analysis. Lü *et al.* (2017) investigated the influence of heating at high temperature on the tensile strength of sandstone by utilizing BD samples, and the main

*Corresponding author, Professor
E-mail: zhemingzhu@hotmail.com

ISSN: 2005-307X (Print), 2092-6219 (Online)

causes for the change of tensile strength of rock have been analyzed.

In the research of rock materials as rock subjected to dynamic loads, many scholars have also been made a great many contributions and achieved many good research results (Cheng *et al.* 2020, Liu *et al.* 2018, Ma *et al.* 2018, Wang *et al.* 2019b, Wu *et al.* 2019). Zhu *et al.* (2015) utilized traditional SHPB equipment to investigate the dynamic mechanical response of Brazilian disk sample under impact loads, and proposed that the dynamic tensile strength of rock materials increases with dynamic loading rates. Wu *et al.* (2016) used granite Brazilian disk samples to conduct dynamic impact test on under hydrostatic pressure, they proposed that the dynamic tensile strength increased with the influence of hydrostatics, and which decreased with the static concentration. Yin *et al.* (2015) studied the changes of the mechanical properties of granite by employing BD samples under different heat treatment conditions, and analyzed the variation of dynamic and static tensile strength. Li *et al.* (2016) investigated the variation of failure patterns and tensile strength with the rate of internal radius to external radius of marble ring samples by static and dynamic splitting tests under different loading rates. In general, these research results have improved the comprehension of the failure behavior of rock materials under different loading condition, and also exposed the importance of the research on the failure modes of rock materials under different loading conditions.

Sandstone has been found extensively as the surrounding rock mass in a real tunnel, which has many special mechanical properties (Zhou *et al.* 2018a, b). The investigation of its mechanical properties not only has greatly theoretical research significance, but also has huge engineering and practical significance. However, there is still a lack of systematic analysis of the dynamic and static mechanical properties of sandstone materials. This research is devoted to study of the failure behavior of three typical types of sandstone materials in geotechnical engineering under impact loads and static loads by employing BD samples, and particular focus is placed on the failure modes of rock materials. The failure properties of different rock materials under the same loading condition was obtained from the simulation, numerical simulation in rock were identified and compared with the experimental results in order to generalize the study of the failure behavior of various rock materials.

2. Experimental process

2.1 Test approach for tensile strength

The splitting tensile strength Brazilian experiment is an indirect tensile estimate approach applied to obtain the tensile strength ($\sigma_{Tensile}$) of the rock materials under static loads and dynamic loads (ISRM 1978, Zhou *et al.* 2011). By using the aboved approach, the BD sample is compressed absolutely to involve a tensile stress state in the sample perpendicular to the loading direction, subsequently results in the failure of the sample. During the Brazilian test, it assumed that the compression and shear strength of the sample is much larger than its tensile strength ($\sigma_{Tensile}$), meanwhile the sandstone materials are homogeneous, isotropic and deforms elastically.

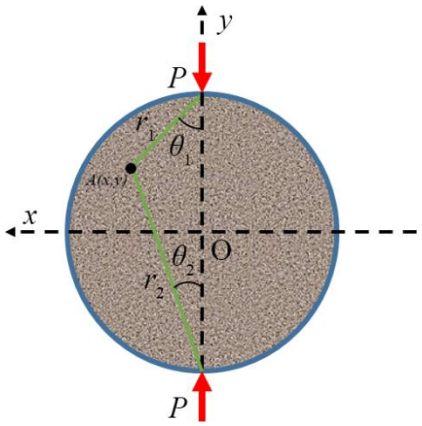

Fig. 1 Sketch map of BD test

According to the linear elastic theory, as a concentrated force (P) is loaded on the disk sample over a very small width like line loading, as shown in Fig. 1, the stress state at one node (A) in the sample can be described as (Jin *et al.* 2017):

$$\sigma_x = \frac{2P}{\pi t}\left[\frac{\sin^2\theta_1\cos\theta_1}{r_1}+\frac{\sin^2\theta_2\cos\theta_2}{r_2}\right]-\frac{2P}{\pi Dt} \quad (1)$$

$$\sigma_y = \frac{2P}{\pi t}\left[\frac{\cos^3\theta_1}{r_1}+\frac{\cos^3\theta_2}{r_2}\right]-\frac{2P}{\pi Dt} \quad (2)$$

$$\tau_{xy} = \frac{2P}{\pi t}\left[\frac{\sin\theta_1\cos^2\theta_1}{r_1}+\frac{\sin\theta_2\cos^2\theta_2}{r_2}\right] \quad (3)$$

With reference to Fig. 1, the σ_x and σ_y denote the stresses at node (A), distance from the node (A) to the loading points can be labeled as r_1 and r_2 at angles θ_1 and θ_2 respectively; D denotes the sample's diameter; t denotes the sample's thickness. At the middle point of the sample, it has $r_1 = r_2 = 0.5D$, the stress state can be expressed by:

$$\sigma_{o,x} = -\frac{2P}{\pi Dt} \quad (4)$$

$$\sigma_{o,y} = \frac{6P}{\pi Dt} \quad (5)$$

These equations illustrate that at the center of the disk's sample, the tensile stress is in the x-axis and the compressive stress is in the y-axis which is three times of the tensile stress and then shear stress disappears along with the diametral plane. As is well known that the compressive strength of rock materials could be an order of magnitude larger than ten times of the tensile strength. The tensile strength can be measured utilizing Eq. (6) for rock materials with elastic characteristics and possessing compression strength larger than its tensile strength:

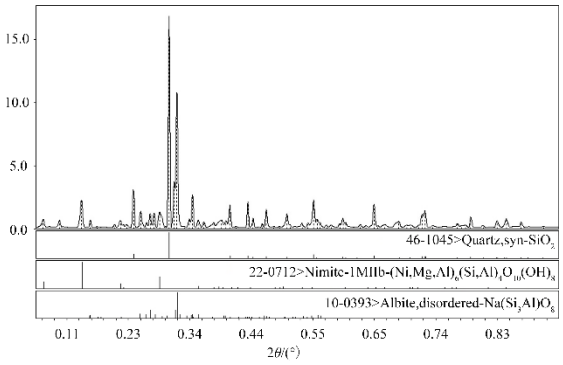

(a) Green sandstone

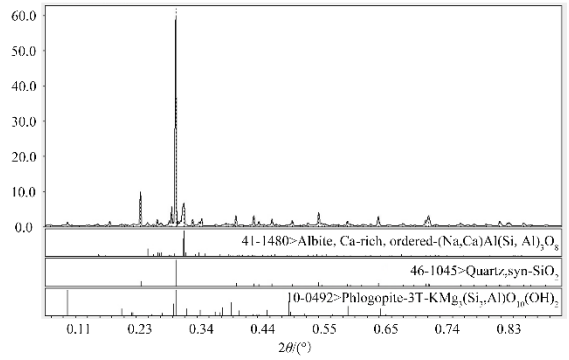

(b) Red sandstone

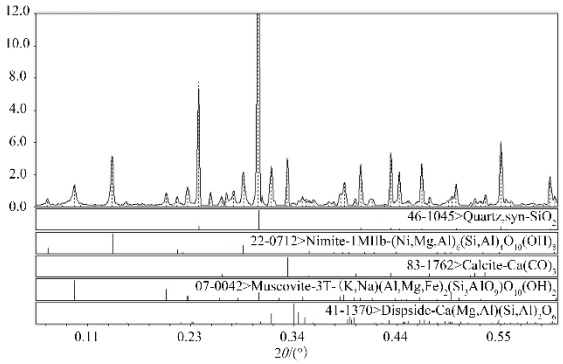

(c) Black sandstone

(d) Results of component analysis

Fig. 2 The experimental results of the component analysis of three sandstone materials

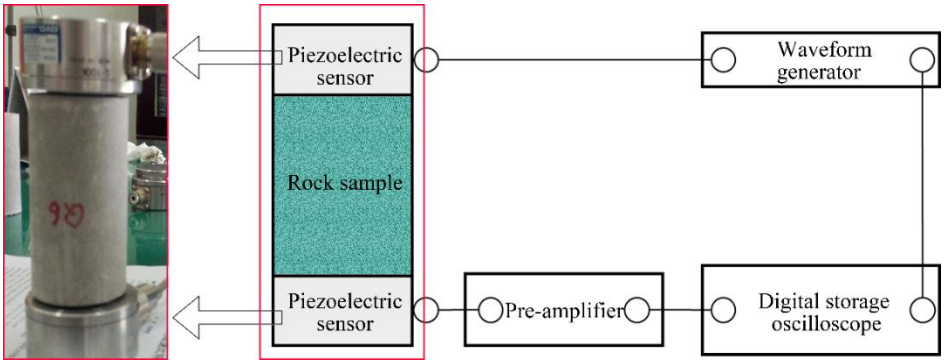

Fig. 3 Measurement of ultrasonic wave velocity

Table 1 The mineralogical composition of the three sandstone materials

Name	Mineralogical composition			
Green sandstone	Quartz	Nimite	Albite	
Red sandstone	Albite	Quartz	Phlogopite	
Black sandstone	Quartz	Nimite	Calcite	DispsideMuscovite

Table 2 Properties of sandstone materials

Properties	Green sandstone	Red sandstone	Black sandstone
Density(kg/m^3)	2265	2443	2596
Static elastic modulus (GPa)	4.5	6.1	11.47
Static Poisson's ratio	0.25	0.25	0.26
Longitudinal wave speed (m/s)	2563.0	2640.7	3954.0
Shear wave speed (m/s)	1607.4	1757.6	2351.1
Rayleigh wave speed (m/s)	1457.6	1603.7	2152.2
Dynamic elastic modulus (GPa)	13.58	15.76	34.79
Dynamic Poisso's ratio	0.164	0.170	0.173

$$\sigma_t = \frac{2P}{\pi Dt} \tag{6}$$

where σ_t represents the tensile strength; P represents the maximum force when the failure occurs.

In the Brazilian experiment, both the static experiment by utilizing the electro-hydraulic servo press and the dynamic experiment by utilizing the SHPB device, respectively, are applied to estimate the tensile strength utilizing the above equation (Zhao and Li 2000).

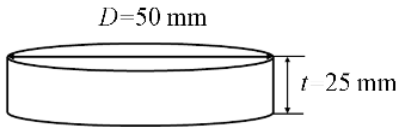

(a) The geometry of BD sample

(b) The picture of BD sample

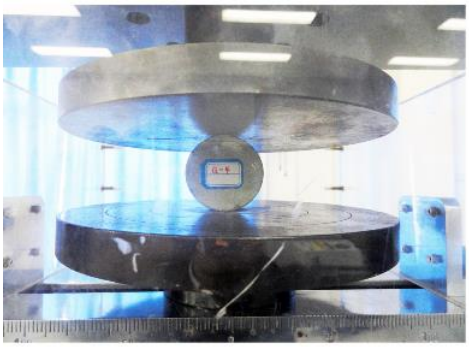

(c) Static loading mode

(d) Test results

Fig. 4 Suggested test approach for the execution of the Brazilian Dick test by ISRM

2.2 Static experiment process

In order to study the variation of tensile strength of three types of sandstone materials under different loading conditions, static splitting test and dynamic splitting test were carried out in laboratory, respectively. The green sandstone, red sandstone and black sandstone in Zigong, Sichuan Province was selected as research objects, and the three types of sandstone materials are sedimentary rocks with isotropic, homogeneous and deforms elastically, these materials have been largely applied to test rock fracture properties (Hua *et al.* 2017, Wang *et al.* 2017, Wang *et al.* 2015).

X-ray diffraction (XRD) was applied to analyze the mineralogical composition of three sandstone materials. The sandstone materials were cut into powder and the fineness was controlled at about 45 microns, i.e. 325 mesh. The experimental results of the mineralogical composition of the three sandstone materials were described in Fig. 2, and are summarized in Table 1. It can be found that Phlogopite is included in red sandstone, this is the reason that red sandstone shows a red rock. It can be also observed that Calcite is the main mineralogical composition of limestone, and it has the property of cementation, thus the dynamic strength of black sandstone may be higher than red and green sandstone.

In this research, the mechanical parameters of sandstone are presented in Table 2. The dynamic elastic modulus (E_d) and the dynamic Poisson ratio (μ_d) for sandstone was computed from the measured dilatational wave speed (c_d) and the measured shear wave speed (c_s) by utilizing the Sonic Viewer-SX ultrasonic testing meter (Yang *et al.* 2018), as shown in Fig. 3. The Poisson ratio (μ_d) of sandstone materials were measured from Wang *et al.* (2011) to measure the shear modulus (G), and Rayleigh wave speed (c_R) can be calculated by Eq. (10):

$$G = \frac{E_d}{1+2\mu_d} \tag{7}$$

$$c_d = \sqrt{\frac{E_d(1-\mu_d)}{\rho(1+\mu_d)(1+2\mu_d)}} \tag{8}$$

$$c_s = \sqrt{\frac{E_d}{2\rho(1+\mu_d)}} \tag{9}$$

$$(2-\frac{c_R^2}{c_s^2}) = 4\sqrt{(1-\frac{c_R^2}{c_d^2})\bullet(1-\frac{c_R^2}{c_s^2})} \tag{10}$$

According to the ISRM suggested methods for the tensile strength tests of rocks, the static and dynamic splitting testing were carried out by employing BD samples. The geometry of the test model is illustrated in Fig. 4(a). The Brazilian disk is a cylinder sample, 50 mm in diameter and 25 mm in thickness. Twelve samples of each sandstone materials were prepared for tests, for a total of 36 BD samples. All sample surfaces must be polished carefully utilizing a grinding machine until the error ranges of the flatness and roughness of every side was less than 0.5 mm and 0.05 mm, respectively. The geometry and picture of all planned green sandstone samples are illustrated in Fig. 4.

2.3 Static experiment results

A series of Brazilian disc static tests loading were conducted using samples prepared from NX size cores, as shown in Fig. 4(c). Before loading, a thin steel wire with a diameter of 1 mm is placed at the both ends of the BD

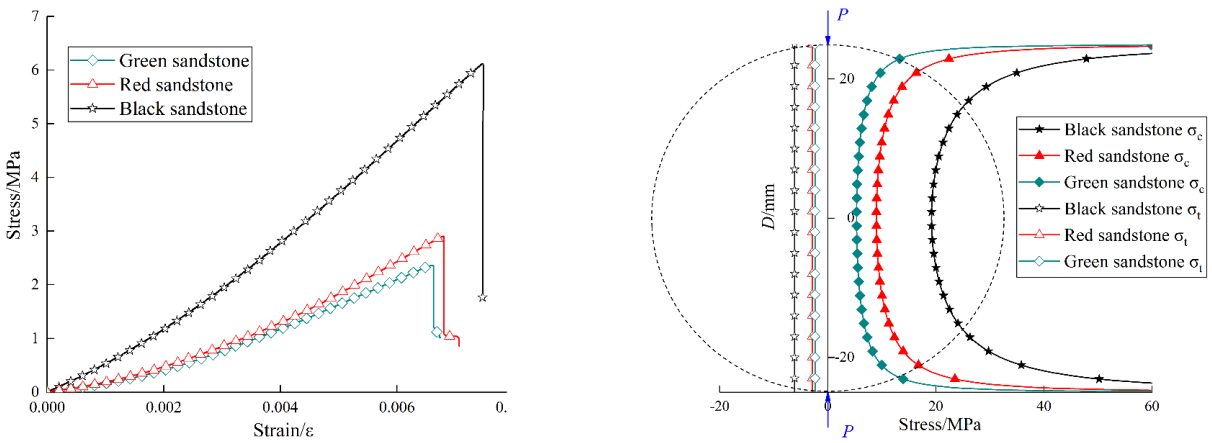

(a) Stress-strain histories of sandstone materials under quasi-static loads (b) Biaxial stress fields distributions of sandstone materials

Fig. 5 Stress-strain histories of sandstone materials under quasi-static loads

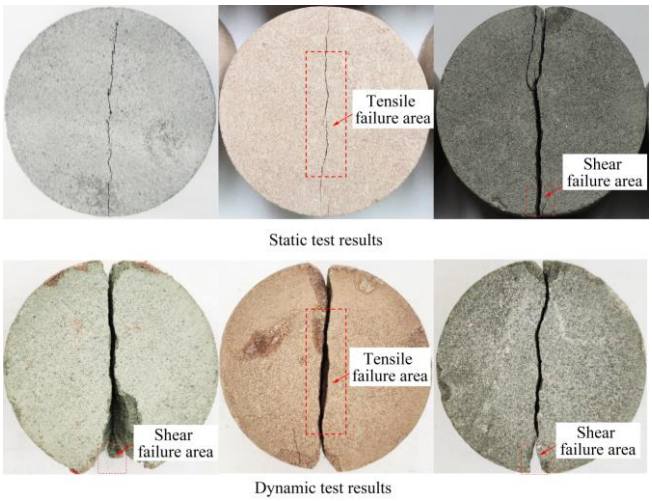

(a) Green sandstone (b) Red sandstone (c) Black sandstone

Fig. 6 Experimental results of sandstone materials

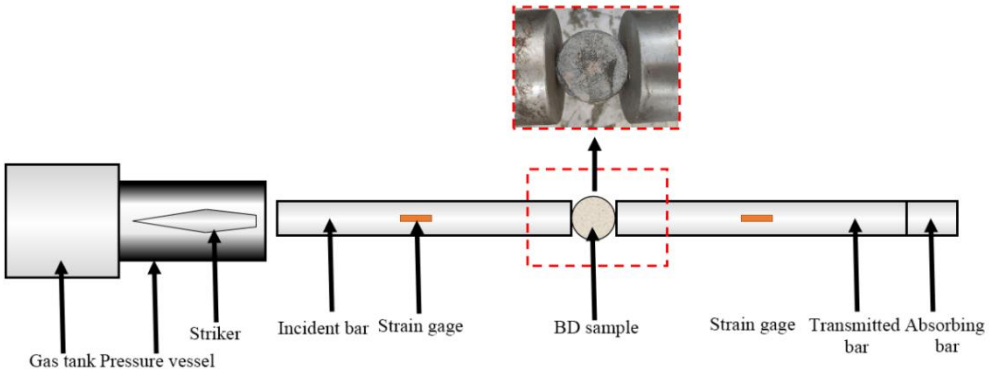

Fig. 7 SHPB test apparatus in this study

samples, so that the loading mode of the sample is close to the linear load. Meanwhile, to prevent the friction effect between the loading plate and the sample from affecting the experiment results, a small amount of Vaseline was smeared on both ends of them. The 30T electro-hydraulic servo press was applied as loading apparatus, and the loading rate of the indirect tests was selected as 0.1 mm/min according to the suggestions of International Society of Rock Mechanics (ISRM). During the experiment, the loads and displacement of each samples were automatically recorded by computer, and then the static tensile strength values of three kinds of rock materials can be obtained according to the stress-strain data from the electro-hydraulic servo press, as shown in Fig. 5(a).

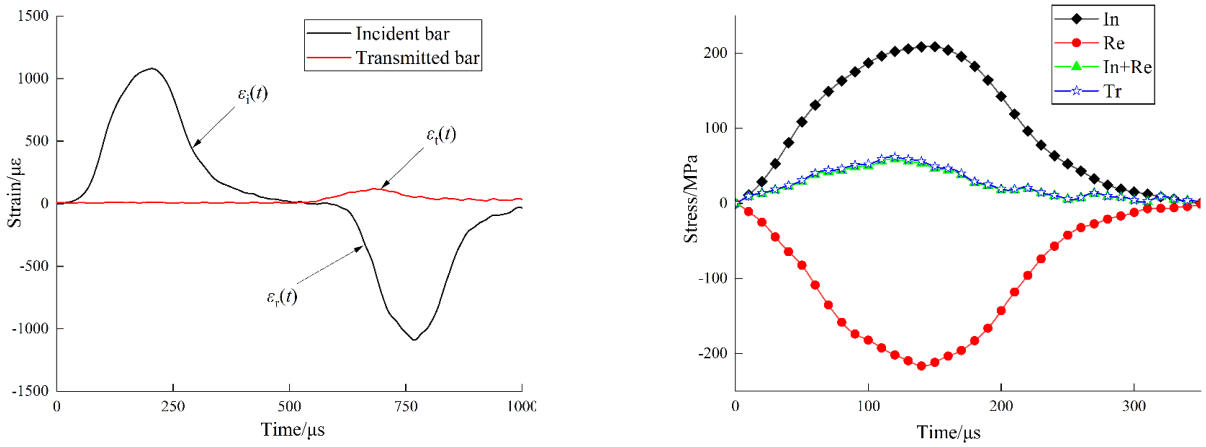

(a) Strain signals versus time (b) Dyanamic loads versus time

Fig. 8 Records of strain signals versus time and records of dynamic loads versus time of black sandstone # 5

From the stress-strain data of the sandstone materials in Fig. 5(a), it can be seen that the sandstone materials obviously perform a kind of brittle material failure characteristics. In this paper, it can be found that the peak stress of black sandstone is obviously larger than that of green sandstone and red sandstone, while the stress peak of red sandstone is slightly larger than that of green sandstone, we can obtain the conclusion that the static tensile strength values of sandstone materials increases with the elastic modulus.

According to Eqs. (4) and (5), the biaxial stresses distribution of Brazilian disk sample can be obtained with diametrically compression, as illustrated Fig. 5(b). One can find that the tensile stress σ_t of sandstone materials is uniformly distributed perpendicular to the radial loading mode (except near the loading head), and the compressive stress σ_c along the radial loading direction presents hyperbolic characteristics, and the center point of the sample is the smallest. The tensile stress of black sandstone is larger than that of the other two sandstones, and the compressive stress of sandstone material is greater than its own tensile stress, which indicates that the compressive strength of sandstone material is larger than that of tensile strength.

As shown in Fig. 5(a) for the experimental results of green sandstone, when stain reaches 0.0066, stress reaches a certain value of 2.26 MPa, and subsequently decrease rapidly because the failure of the sample. It can see from Fig. 6 (Static test results), a main flaw develops quickly in the middle region. Besides, no small flaws can be observed on the surface of the sample for green sandstone and red sandstone, but some tiny flaws can be observed on the surface of the sample for black sandstone.

2.4 Dynamic experiment process

A schematic diagram of a traditional SHPB apparatus is illustrated in Fig. 7. A BD sample was placed between incident and transmitted bars. A striker, of the same material as the incident bar, was applied to impinge upon the incident bar. The incident and transmitted bars are made of 42CrMo with a density of 7850 kg/m^3 and elastic modulus of 210 GPa.

Impact of the area at the free end of the incident bar produces a stress compressive pulse $\varepsilon_i(t)$, and a typical test data is obtained, as illustrated in Fig. 8. When the stress compressive pulse reaches the sample interface, one part of it, $\varepsilon_r(t)$, will be reflected, and remaining part passes through the whole sample and enters into the transmitted bar as the transmitted pulse $\varepsilon_t(t)$. The stress pulses were collected by strain gauges stuck at the center of the incident and transmitted bars, as shown in Fig. 8(a).

Based on one-dimensional elastic wave hypothesis of a cylindrical bar with a length much larger than its lateral dimension, the idealized stress pulse equation can be described by:

$$\rho \frac{d^2}{dt^2} u = E_e \bullet \frac{d^2}{dx^2} u \tag{11}$$

where ρ represents density of the elastic bars; E_e represents the elastic modulus of the elastic bars; u represents the displacement in the x-direction; t represents the time.

The hypothesis of uniform stress on the sample means that the stress at the incident bar/sample interface is equal to that at the sample/transmitted bar interface, i.e.,

$$\sigma_i(t) + \sigma_r(t) = \sigma_t(t) \tag{12}$$

where $\sigma_i(t)$ represents the compressive incident stress versus time; $\sigma_r(t)$ represents the compressive reflected stress versus time; $\sigma_t(t)$ represents the compressive transmitted stress versus time.

Therefore, Eq. (15) also can be described as:

$$\sigma(t) = \frac{A_e E_e}{A_S} \cdot \varepsilon_t(t) \tag{13}$$

$$\varepsilon(t) = -2\frac{C_e}{L_S} \cdot \int_0^t [\varepsilon_r(t)] dt \tag{14}$$

Table 3 Tensile test results of sandstone materials

Material		Strain rate/s $^{-1}$	Static tensile strength /MPa	Strain rate/s $^{-1}$	Dynamic tensile strength /MPa	S
Green sandstone	#1	1.67×10^{-5}	1.985	220.72	23.712	11.945
	#2	1.67×10^{-5}	2.172	236.89	22.338	10.284
	#3	1.67×10^{-5}	2.013	230.65	18.476	9.178
	#4	1.67×10^{-5}	2.216	236.63	28.592	12.902
	#5	1.67×10^{-5}	1.935	223.98	20.407	10.546
	#6	1.67×10^{-5}	2.203	213.12	25.465	11.559
Red sandstone	#1	1.67×10^{-5}	3.071	208.95	30.935	10.073
	#2	1.67×10^{-5}	3.251	234.75	32.763	10.077
	#3	1.67×10^{-5}	3.121	211.08	37.167	11.908
	#4	1.67×10^{-5}	2.936	195.93	23.134	7.879
	#5	1.67×10^{-5}	3.329	232.07	23.967	7.199
	#6	1.67×10^{-5}	2.957	194.96	30.571	10.338
Black sandstone	#1	1.67×10^{-5}	6.426	236.18	55.209	8.591
	#2	1.67×10^{-5}	6.831	234.66	47.868	7.007
	#3	1.67×10^{-5}	6.118	235.83	39.169	6.402
	#4	1.67×10^{-5}	6.072	236.63	69.600	11.462
	#5	1.67×10^{-5}	7.235	236.62	58.734	8.118
	#6	1.67×10^{-5}	7.383	236.31	54.384	7.366

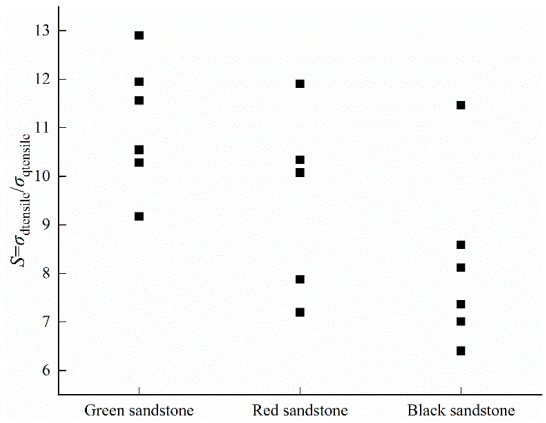

Fig. 9 The tensile sensitivity coefficient of sandstone material

$$\frac{d\varepsilon(t)}{dt} = -2\frac{C_e}{L_S}\cdot\varepsilon_r(t) \tag{15}$$

2.5 Dynamic experiment results

From Fig. 8(b), it can be observed that the transmission stress wave is coincide with the sum of the incident and reflected pulses, especially in the rising region of the loads histories. It can be found that the stress balance can be reached. Then, according to the loads peak value of the sum of the incident pulse and the reflected pulse, the maximum value can be considered as the dynamic tensile strength of sandstone materials. The dynamic tensile strength values of three types of sandstone materials can be obtained, which were listed in Table 3.

The tensile sensitivity coefficient S is defined as the rate of the dynamic tensile strength $\sigma_{dtensile}$ to the static tensile strength $\sigma_{stensile}$, and this can be described as:

$$S = \frac{\sigma_{dtensile}}{\sigma_{stensile}} \tag{16}$$

The tensile sensitivity coefficients of each group of sandstone materials were illustrated in Fig. 9. It is found that green sandstone material is the most sensitive to the strain rate, while the black sandstone is the least sensitive to the strain rate. It can be also observed that dynamic tensile strength is approximately ten times than static tensile strength for sandstone materials.

3. Numerical simulation

3.1 Simulation under static loads

In order to clearly understand the failure behavior of BD samples under static loads, a series of finite element numerical models were established by utilizing RFPA2D computer program (Niu *et al.* 2017, Wang *et al.* 2016b, Wang *et al.* 2014). In the finite element program of RFPA2D, it is assumed that some rigid circular particles joined together which simulate the interaction relation between gains of rock. Because the rock materials in simulation models may undergo tensile or shear failure, and therefore in these simulation models, two criteria, i.e., maximum tensile stress criterion and Mohr-Coulomb criterion were applied to judging element stability. According to these two criteria, when the maximum tensile strain or shear stress exceeds the corresponding limit, the element fails. The maximum tensile stress criterion can be described as:

$$\sigma_1 \geq \sigma_t \tag{17}$$

where σ_1 represents the maximum principal stress; σ_t represents the uniaxial tensile strength.

The Mohr-Coulomb criterion can be described as:

$$\sigma_1 = \frac{1+\sin\phi}{1-\sin\phi}\bullet\sigma_3 + \frac{2C}{1-\sin\phi} \tag{18}$$

where σ_1 denotes the maximum principal stress; σ_3 denotes the minimum principal stress; ϕ denotes the internal friction angle; C denotes the internal cohesion.

The elastic modulus E will be attenuated after an element is damaged, and it can be described as:

$$E = (1-\omega)E_0 \tag{19}$$

where ω represents damage modulus, E_0 represents the initial elastic modulus, E represents the elastic modulus after damage.

3.2 Simulation results of static loads

To achieve the same loading conditions as the

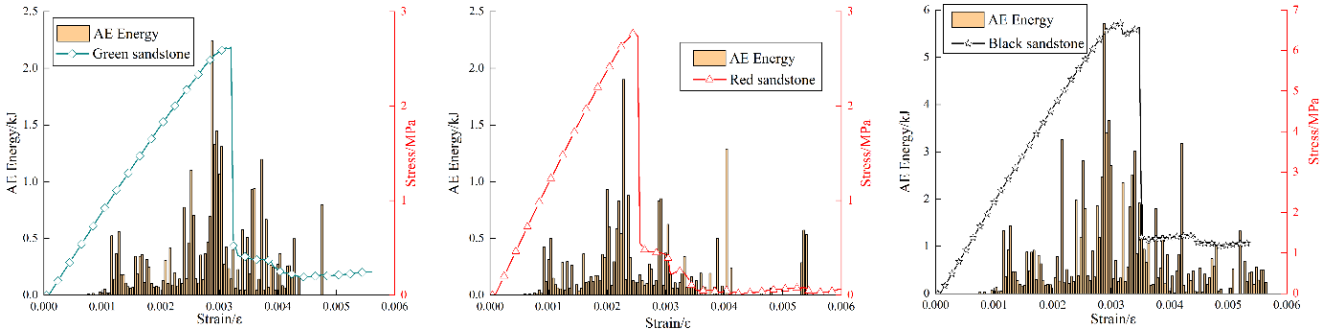

(a) Green sandstone (b) Red sandstone (c) Black sandstone

Fig. 10 Acoustic emission (AE) energy distributions and stress-strain data

Table 4 Error analysis

Material	Test results (average value) $\sigma_{stensile}$ /MPa	Numerical results (average value) $\sigma_{stensile}$ /MPa	Error/%
Green sandstone	2.090	2.316	9.87
Red sandstone	3.111	2.839	9.57
Black sandstone	6.677	6.571	1.62

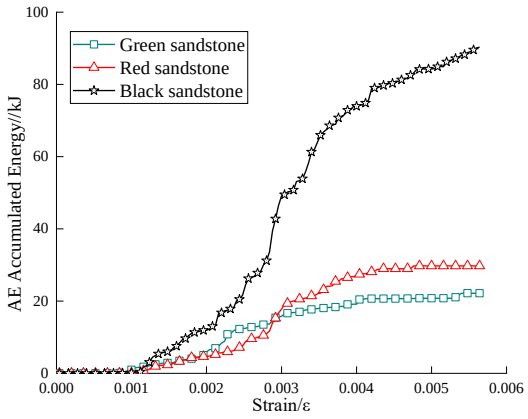

Fig. 11 Distribution of acoustic emission accumulated energy

experimental loads, the loading plots as illustrated in Fig. 5 were applied as the boundary conditions of the simulation models, and the acoustic emission (AE) energy distributions and stress-time plots under static loads can be obtained from simulation results, as illustrated in Fig. 10. It can be observed that the maximum AE energy occurs before the maximum failure stress peak value, the maximum failure mode of the sample occurs before the maximum loading force. The peak stress values of the numerical simulation are 2.316 MPa, 2.839 MPa and 6.571 MPa, respectively, and the error is 9.87% for green sandstone, 9.57% for red sandstone, and 1.62% for black sandstone, respectively, as illustrated in Table 4. From the stress-time plots, it can be seen that the three types of sandstone materials perform brittle failure characteristics. As the stress reaches its peak value, the sample has been completely failed. It can also be observed that the initial damage of green and red sandstone begins to occur at the strain 6.0×10^{-6} and 7.6×10^{-6}, while the initial damage of black sandstone begins to occur at the strain 7.6×10^{-6}. It indicates that the tensile strength of green sandstone is smaller than that of black and red sandstone under same loading conditions.

According to the distributions of AE energy distributions, the AE accumulative energy distributions of sandstone materials can be obtained, as shown in Fig. 11. The AE accumulative energy of green sandstone is the smallest, while that of black sandstone is the largest. As the loading step reaches between 0.0024 and 0.0032, the AE accumulative energy of sandstone material increases sharply, which indicates that the maximum damage occurs at this time, and which is coincide with simulation results in Fig. 12.

Acoustic emission damage distributions (red ring indicates tensile damage, white ring indicates shear damage) and maximum principal stress damage distributions can be obtained from numerical simulation results, as illustrated in Fig. 12. For green sandstone, tensile failure begins to occur at Step=14 ($\varepsilon=6.0\times10^{-6}$), and then shear damage begins to occur at Step=19 ($\varepsilon=7.6\times10^{-6}$), and subsequently the failure of disc samples is accompanied by the joint failure of tension and shear. It can be seen that tensile failure plays a dominant role in the fracture behavior. The initial tensile damage of disc samples occurs at the middle of the disc, which is basically coincide with research results of other researchers (Huang *et al.* 2016; Li and Wong 2012). However, for black sandstone, the tensile failure begins to occur at Step=19 ($\varepsilon=7.6\times10^{-6}$), followed by shear damage at Step=24 ($\varepsilon=9.6\times10^{-6}$), which lags behind that of the green sandstone samples.

3.3 Simulation under dynamic loads

To simulate the actual impact process, several finite difference simulation models of the whole SHPB equipment under impact loads were built by employing AUTODYN code in the present study. The numerical models were designed according to the dimensions, the boundary and the loading conditions. Two-dimensional quadrilateral elements were used to mesh the whole sample, and the number of elements is 160000. Fig. 13 shows a scaled close-up view of a typical mesh for parts of the incident and transmitted bars and the sample. The bottom of the concrete amortisseur was established as the no-reflection boundary, which can minimise the influence of the reflected stress wave on fracture behavior. The crack width is established according to the experimental models, and the mechanical parameters

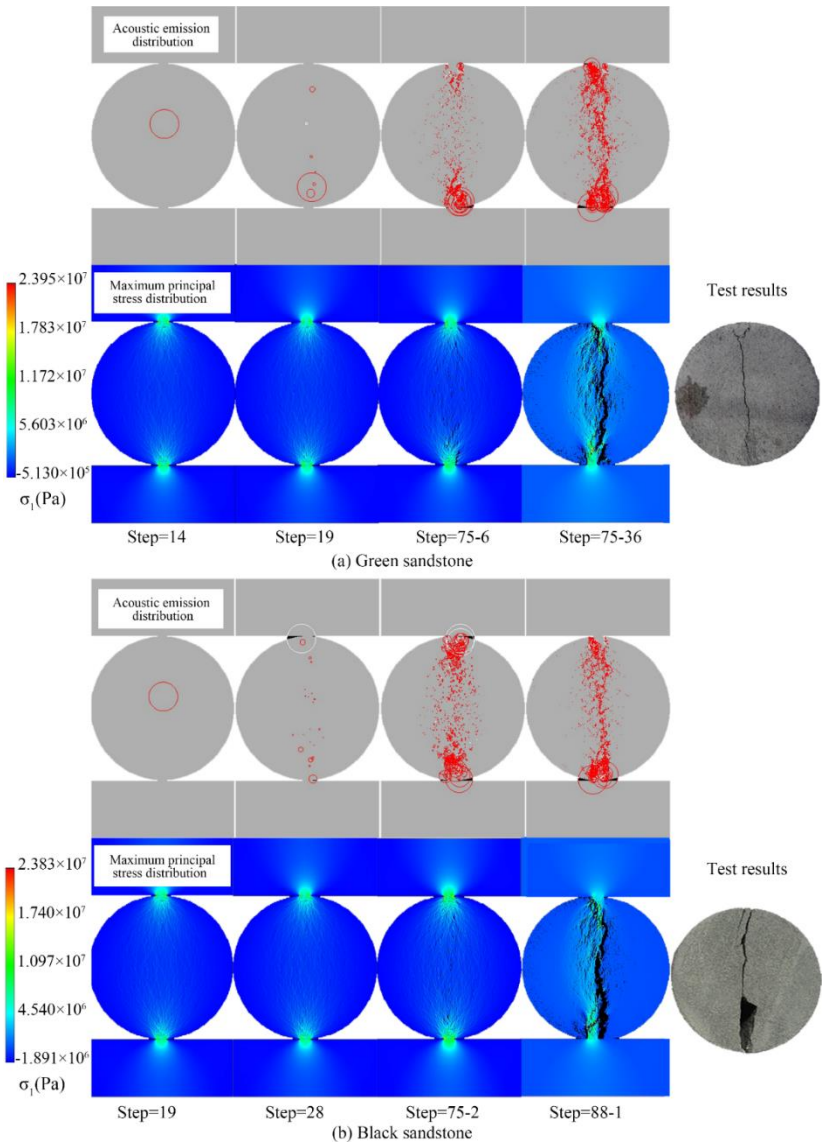

Fig. 12 Acoustic emission distribution and maximum principal stress distribution during BD sample failure

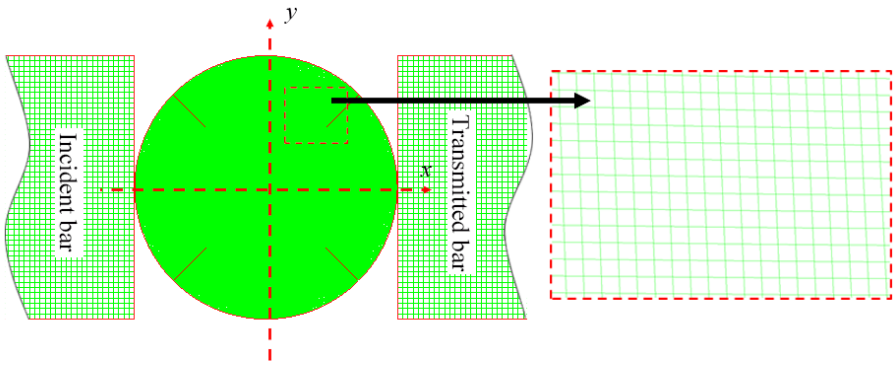

Fig. 13 Mesh picture of the BD sample in numerical model

of four types of brittle materials applied in this simulation are listed in Table 2.

In the process of the impact testing, the pressure or deformation is relatively small, thus the density or volumetric deformation of the brittle material is linearly related to the pressure. Thus, the linear equation of state (EOS) is adopted (Tham 2005, Wong and Li 2013):

$$P=\kappa\mu=\kappa\left(\frac{\rho}{\rho_0}-1\right) \tag{20}$$

where P represents pressure, κ represents bulk modulus, ρ represents density and ρ_0 represents original density.

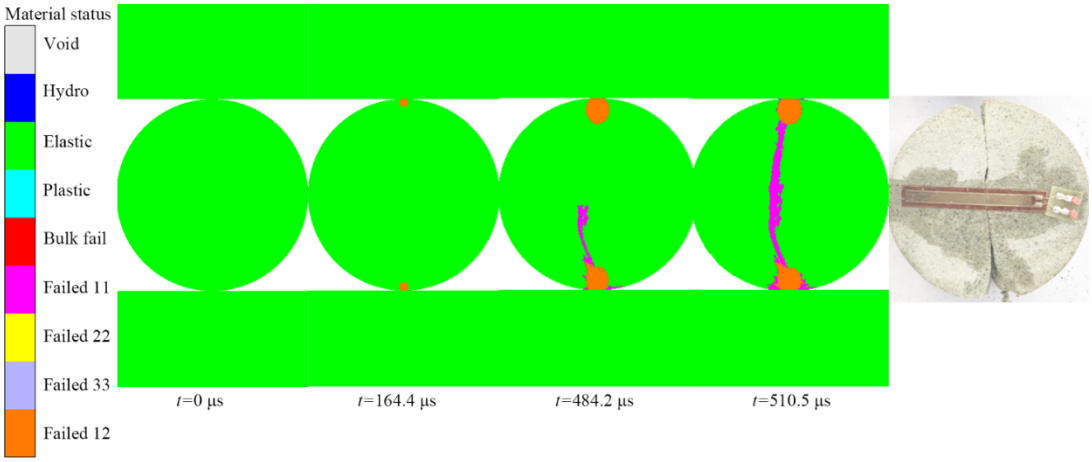

Fig. 14 Numerical simulation results under impact loading

Failure criteria plays a key role in dynamic numerical models, which describe material status under dynamic loads. Except for the sample, there was no failure for all the parts of the impact system. Thus, no failure criterion was employed to them. For the sandstone samples, the major principal stress failure criterion is adopted in this study to describe the progressive failure. As the maximum tensile or the maximum shear stress exceed the tensile or shear strength of brittle materials, the element fails, i.e. (Jiang *et al.* 2014, Jiang *et al.* 2017)

$$\sigma_1 \geq [\sigma] \text{ or } \tau_{12} \geq [\tau_r] \tag{21}$$

where σ_1 represents maximum tensile principal stress, $[\sigma]$ represents tensile strength, τ_{12} represents maximum shear stress, and τ_r represents shear strength. In the numerical simulation, as an element fails, it will can't stand any tensile and shear loads, but the element still be able to stand compressive loads.

3.4 Simulation results of impact loads

The failure behavior for the green sandstone sample versus time were illustrated in Fig. 15. In general, the numerical simulation results are coincide with our dynamic experimental results. In the simulation results, shear failure begins first, followed by tensile failure, and the proportion of tensile failure is greater than that of shear failure. The shear failure symmetry occurs at the two loading ends of the BD sample, and the tensile failure occurs at the center region of the BD sample, and a new crack develops on the central axis. According to the failure regions of the pixels in Fig. 15, the rates of tensile failure and shear failure are 54.92% and 45.08%, respectively, which indicates that tensile failure also accounts for most of the dynamic failure process.

4. The microstructure of failure surface

In a polycrystalline material, the fracture surfaces observed by employing scanning electron microscope (SEM) can be divided into two categories: Transgranular (TG) microcracks (through the grain) and intergranular (IG) microcracks (along the grain boundaries), they are two main characteristics of fracture between rock particles (Zhang and Zhao 2013). Zhang and Zhao (2014) proposed that TG fracture dissipates more energy than IG fracture does in the failure process of rock. Thus, the ratio of TG fracture in sandstone is larger than the IG fracture under dynamic loads, but the ratio of IG fracture in sandstone is larger than the TG fracture under static loads. Fig. 15 illustrates the microstructures of fracture patterns of three kinds of sandstone BD samples observed by SEM under dynamic loads. When the fracture surfaces have been amplified to 500 times, the microstructures of sandstone particles was observed by SEM. The fracture surface of the three types of sandstones are rough, which indicates that TG fracture was the most failure form in the fracture surface of green sandstone, meanwhile there exists a small amount of IG fractures. The results show that the strength of black sandstone crystal is the largest, the energy to cause TG fracture is the largest, and the ability to resist micro-crack initiation is the largest, which also makes the dynamic tensile strength of black sandstone the highest. This is consisted with the previous study (Dumont *et al.* 2004, Yang *et al.* 1991).

When the fracture surfaces were amplified to 10000 times, it can be observed that the porosity of the green sandstone is largest than that of the other two sandstones. The particles destruction of the green sandstone was mainly IG under dynamic loads, and therefore the tensile strength value of the black sandstone is much larger than the other two sandstones.

4.1 Calculation of the fractal dimension

Fractal geometry has been widely used to describe irregular and disorderly phenomena and behavior (Mandelbrot 1967). The fractal dimension of rock fracture distribution is a comprehensive reflection of rock microstructure, loading mode and sample size. Therefore, the fractal dimension was computed in this study.

A great many methods have been adopted for computing the fractal dimension of materials fracture surface at

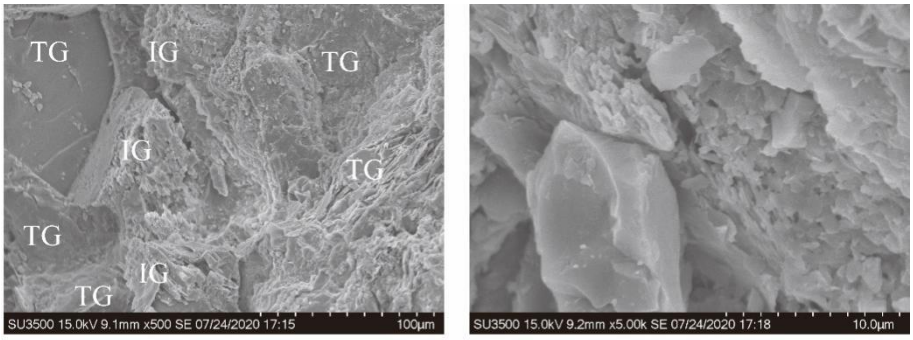

(a) Green sandstone

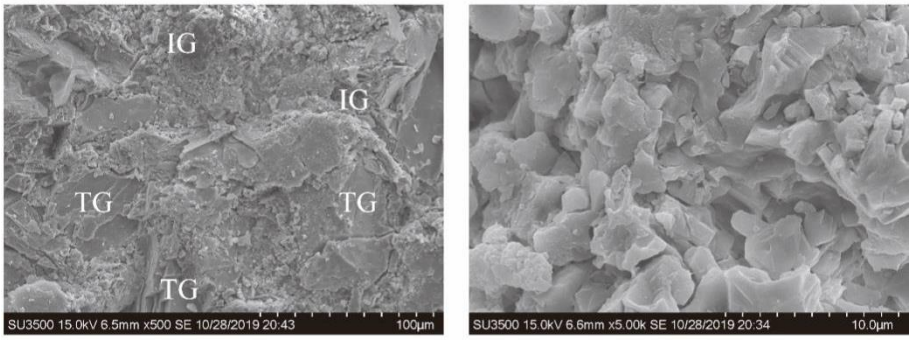

(b) Red sandstone

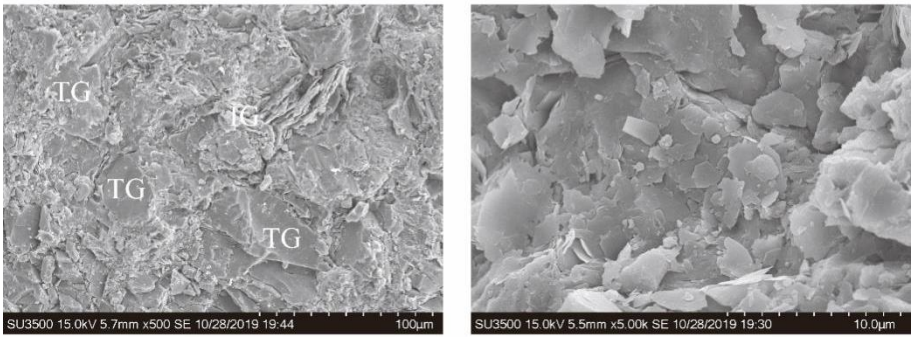

(c) Black sandstone

Fig. 15 The microstructures of sandstone scanned by SEM

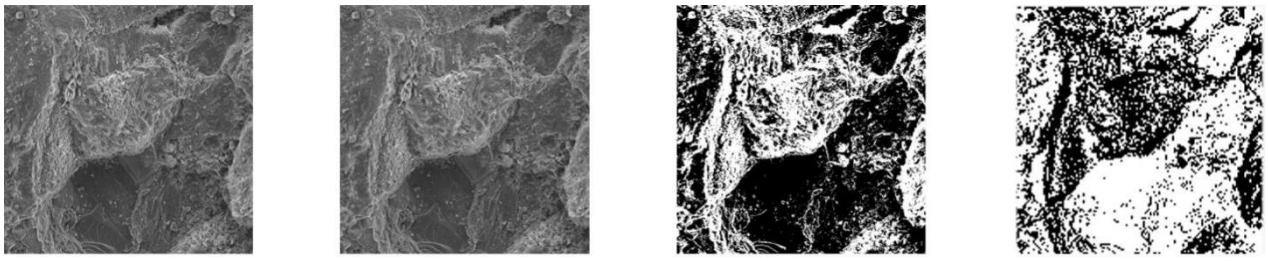

(a) Originial image (b) Gray image (c) Binary image (d) Reverse binary image

Fig. 16 Crack image extraction process of SEM images for green sandstone

microstructure, such as perimeter-area relationship method (Florio *et al.* 2019), self-affine fractal method (Wang *et al.* 2016a), box dimension method (Rabal *et al.* 2018) and Hausdroff dimension method (Liu and Sun 2017), etc. The box dimension method is relatively intuitive, easy to calculation by MATALAB code, and the geometric self-similarity requirement of the image is not very strict, which has been widely applied in many research achievements, and thus this study chooses the box dimension method to compute the fractal dimension.

The box dimension fractal method can be defined as: there are a large number of closed boxes with length δ, which are arranged in an orderly manner over the existing binary images, and these boxes do not overlap with each other. The boxes containing black contents are counted and the total number is $N(\delta)$. When δ tends to zero, the limit value is the box dimension fractal dimension D, the box fractal dimension for that threshold is obtained by using the

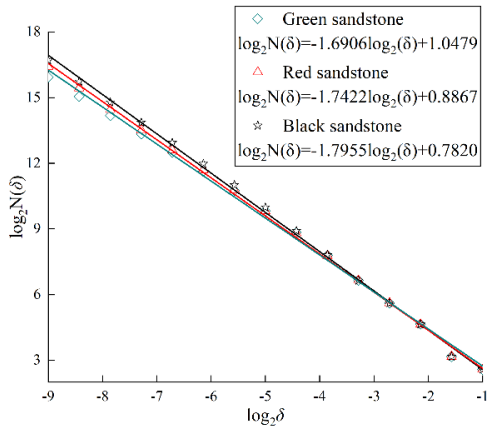

(a) Fractal dimension calculation in box counting

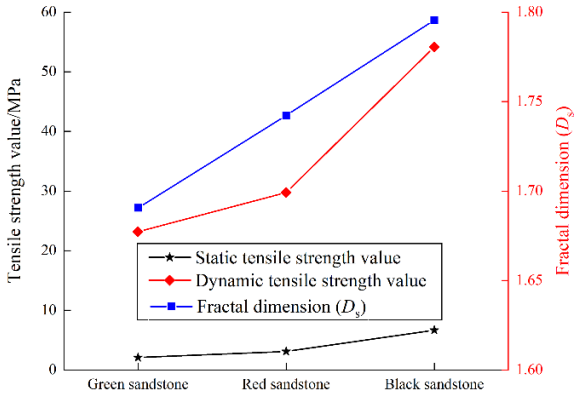

(b) Relationship between fractal dimension and tensile strength

Fig. 17 The distributions of the fractal dimension of sandstone materials

expression:

$$D = \lim_{\delta \to 0} \frac{\log N(\delta)}{\log(\frac{1}{\delta})} \tag{22}$$

where D denotes the fractal dimension; δ denotes the size of the box.

In application, the length of the box only reaches a limited value, the least square method is usually used to fit the curve, which can be described as:

$$\log N(\delta) = D_s \log(\frac{1}{\delta}) + B \tag{23}$$

where D_s denotes the value of fractal dimension.

According to the above fractal box dimension calculation approach, the fractal box dimension of the binary image was computed by using MATLAB code. The binary image processed from SEM image is composed of a series of pixels, which can be regarded as a numerical matrix of $m \times n$. In this image, a pixel is taken as the smallest box, and 512×512 pixel regions are selected, the number of boxes containing black pixels in different scales is counted, and the corresponding relationship between $\log_2 N(\delta)$ and $\log_2(1/\delta)$ can be obtained, as shown in Fig. 17(a).

According to the theory of the fractal dimension, the larger value of the fractal dimension, the more complicated the fracture is, and the greater the energy consumed to produce the fracture per unit area at macro level, and the higher the energy required for fracturing. Thus, we can know that from Fig. 17(b), the fractal dimension for black sandstone is 1.7955, for red sandstone is 1.7422, for green sandstone is 1.6906, respectively. It can be observed that the tensile strength value of sandstone is proportional to the fractal dimension, and we can conclude that the fractal dimension can be used as the criterion of dynamic tensile strength judgement.

5. Conclusions

The tensile strength and the failure behavior of three types of sandstone materials taken from Sichuan province were obtained by conducting the static and dynamic splitting tests. The main causes for the difference in tensile strength values and fracture modes were discussed and analyzed, and the corresponding simulation was conducted by using the finite element code and the finite difference code, and subsequently we come to the following significantly conclusions:

• The static and dynamic tensile strength of black sandstone are both much larger than those of green sandstone and red sandstone, the static tensile strength of green sandstone is about 31.30% of black sandstone, the dynamic tensile strength of green sandstone is about 42.77% of black sandstone.

• The tensile failure plays a significant role in the failure mode of sandstone materials under both dynamic and static loads, shear failure also occurs in the process of failure. The failure modes of BD samples are mainly developed from the middle to both ends, and finally it splits and breaks in half, and the time of maximum damage in sandstone under static loads is preceded by the time of maximum stress value.

•The mineralogical composition strength in sandstone is the mainly determining factor for the tensile strength, TG fracture predominates in green sandstone failure behavior under dynamic loading. The tensile strength value is proportional to the fractal dimension by employing MATLAB code, the fractal dimension can be used as the preliminary judgement of the tensile strength.

Acknowledgments

This work was financially supported by the National Natural Science Foundation of China (U19A2098); the project of Science and Technology of Sichuan province (21YYJC2845); Open fund of Key Laboratory of Deep Underground Science and Engineering (DESE202005); the Fundamental Research Funds for the Central Universities.

References

Bahaaddini, M., Serati, M., Masoumi, H. and Rahimi, E. (2019),

"Numerical assessment of rupture mechanisms in Brazilian test of brittle materials", *Int. J. Solids Struct.*, **180**, 1-12. https://doi.org/10.1016/j.ijsolstr.2019.07.004.

Cheng, Y., Song, Z., Jin, J., Wang, T. and Yang, T. (2020), "Waveform characterization and energy dissipation of stress wave in sandstone based on modified SHPB tests", *Geomech. Eng.*, **22**(2), 187-196. https://doi.org/10.12989/gae.2020.22.2.187.

Dumont, D., Deschamps, A. and Brechet, Y. (2004), "A model for predicting fracture mode and toughness in 7000 series aluminium alloys". *Acta Mater.*, **52**(9), 2529-2540. https://doi.org/10.1016/j.actamat.2004.01.044.

Feng, J., Wang, E., Shen, R., Chen, L., Li, X. and Xu Z. (2016), "Investigation on energy dissipation and its mechanism of coal under dynamic loads", *Geomech. Eng.*, **11**(5), 657-670. https://doi.org/10.12989/gae.2016.11.5.657.

Florio, B.J., Fawell, P.D. and Small, M. (2019), "The use of the perimeter-area method to calculate the fractal dimension of aggregates", *Powder Technol.*, **343**, 551-559. https://doi.org/10.1016/j.powtec.2018.11.030.

Haeri, H., Shahriar, K., Marji, M.F. and Moarefvand P. (2014), "Experimental and numerical study of crack propagation and coalescence in pre-cracked rock-like disks", *Int. J. Rock Mech. Min. Sci.*, **67**, 20-28. https://doi.org/10.1016/j.ijrmms.2014.01.008.

Hang, L., Wei, X. and Yan, Q. (2016), "Modified formula for the tensile strength as obtained by the flattened Brazilian disk test", *Rock Mech. Rock Eng.*, **49**(4), 1579-1586. https://doi.org/10.1007/s00603-015-0785-z.

Hua, W., Dong, S., Fan, Y., Pan, X. and Wang, Q. (2017), "Investigation on the correlation of mode II fracture toughness of sandstone with tensile strength", *Eng. Fract. Mech.*, **184**, 249-258. https://doi.org/10.1016/j.engfracmech.2017.09.009.

Huang, Y., Yang, S., Ju, Y., Zhou, X. and Zhao, J. (2016), "Study on particle size effects on strength and crack coalescence behavior of rock during Brazilian splitting test", *J. Cent. South Univ.*, **47**(4), 1272-1281. https://doi.org/10.11817/j.issn.1672-7207.2016.04.025.

Huang, Y.G., Wang, L.G., Lu, Y.L., Chen, J.R. and Zhang, J.H. (2015), "Semi-analytical and numerical studies on the flattened brazilian splitting test used for measuring the indirect tensile strength of rocks", *Rock Mech. Rock Eng.*, **48**(5), 1849-1866. https://doi.org/10.1007/s00603-014-0676-8.

ISRM (1978), "International society for rock mechanics commission on standardization of laboratory and field tests", *Int. J. Rock Mech. Min. Sci. Geomech. Abstr.*, **15**(6), 319-368. https://doi.org/10.1016/0148-9062(78)91472-9.

Jiang, H., Du, C. and Liu, Z. (2017), "Theoretical and numerical investigation on rock fragmentation under high-pressure water-jet impact", *Iran. J. Sci. Technol. T. Civ. Eng.*, **41**(3), 305-315. https://doi.org/10.1007/s40996-017-0065-0.

Jiang, H., Du, C., Liu, S. and Gao, K. (2014), "Numerical simulation of rock fragmentation under the impact load of water jet", *Shock Vib.*, 1-11. http://doi.org/10.1155/2014/219489.

Jin, X., Hou, C., Fan, X., Lu, C., Yang, H., Shu, X. and Wang, Z. (2017), "Quasi-static and dynamic experimental studies on the tensile strength and failure pattern of concrete and mortar discs", *Sci. Rep.*, **7**(1), 15305. https://doi.org/10.1038/s41598-017-15700-2.

Li, D. and Wong, L.N.Y. (2013), "The Brazilian disc test for rock mechanics applications: review and new insights", *Rock Mech. Rock Eng.*, **46**(2), 269-287. https://doi.org/10.1007/s00603-012-0257-7.

Li, D., Tao, W., Cheng, T. and Sun, X. (2016), "Static and dynamic tensile failure characteristics of rock based on splitting test of circular ring", *T. Nonferr. Metal Soc.*, **26**(7), 1912-1918. https://doi.org/10.1016/S1003-6326(16)64307-8.

Li, H. and Wong, L.N.Y. (2012), "Influence of flaw inclination angle and loading condition on crack initiation and propagation", *Int. J. Solids Struct.*, **49**(18), 2482-2499. https://doi.org/10.1016/j.ijsolstr.2012.05.012.

Liu, C., Deng, H., Zhao, H. and Zhang, J. (2018), "Effects of freeze-thaw treatment on the dynamic tensile strength of granite using the Brazilian test", *Cold Reg. Sci. Technol.*, **155**, 327-332. https://doi.org/10.1016/j.coldregions.2018.08.022.

Liu, Q. and Sun, W. (2017), "A Hilbert-type fractal integral inequality and its applications", *J. Inequal. Appl.*, (1), 1-8. https://doi.org/10.1186/s13660-017-1360-9.

Lü, C., Sun, Q., Zhang, W., Geng, J., Qi, Y. and Lu, L. (2017), "The effect of high temperature on tensile strength of sandstone", *Appl. Therm. Eng.*, **111**, 573-579. https://doi.org/10.1016/j.applthermaleng.2016.09.151.

Ma, T., Peng, N., Zhu, Z., Zhang, Q., Yang, C. and Zhao, J. (2018), "Brazilian tensile strength of anisotropic rocks: Review and new insights", *Energies*, **11**(2), 1-25. https://doi.org/10.3390/en11020304.

Mandelbrot, B. (1967), "How long is the coast of Britain? Statistical self-similarity and fractional dimension", *Science*, **156**, 636-638. https://doi.org/10.1126/science.156.3775.636.

Nezhad, M.M., Fisher, Q.J., Gironacci, E. and Rezania, M. (2018), "Experimental study and numerical modeling of fracture propagation in shale rocks during brazilian disk test", *Rock Mech. Rock Eng.*, **51**(6), 1755-1775. https://doi.org/10.1007/s00603-018-1429-x.

Niu, L., Zhu, W., Cheng, Z., Guan, K. and Qin, T. (2017), "Numerical simulation on excavation-induced damage of rock under quasi-static unloading and dynamic disturbance", *Environ. Earth Sci.*, **76**, 613-627. https://doi.org/10.1007/s12665-017-6955-4.

Rabal, H., Grumel, E., Cap, N., Buffarini, L. and Trivi, M. (2018), "A descriptor of speckle textures using box fractal dimension curve", *Opt. Laser Eng.*, **106**, 47-55. https://doi.org/10.1016/j.optlaseng.2018.02.006.

Sarfarazi, V., Haeri, H., Marji, M.F. and Zhu, Z. (2017), "Fracture mechanism of brazilian discs with multiple parallel notches using PFC2D", *Period Polytech. Civ.*, **61**(4), 653-663. https://doi.org/10.3311/PPci.10310.

Sheikh, M.Z., Wang, Z., Bing, D., Suo, T., Li, Y., Zhou, F., Wang, Y., Dar, U.A., Gao, G. and Wang, Y. (2019), "Static and dynamic brazilian disc tests for mechanical characterization of annealed and chemically strengthened glass", *Ceram. Int.*, **45**(6), 7931-7944. https://doi.org/10.1016/j.ceramint.2019.01.106.

Tham, C.Y. (2005), "Reinforced concrete perforation and penetration simulation using AUTODYN-3D", *Finite Elem. Anal. Des.*, **41**(14), 1401-1410. https://doi.org/10.1016/j.finel.2004.08.003.

Wang, M., Chen, Y., Ma, G., Zhou, J. and Zhou, C. (2016a), "Influence of surface roughness on nonlinear flow behaviors in 3D self-affine rough fractures: Lattice Boltzmann simulations", *Adv Water Resour.*, **96**, 373-388 .https://doi.org/10.1016/j.advwatres.2016.08.006.

Wang, M., Wang, F., Zhu, Z., Dong, Y., Mousavi Nezhad, M. and Zhou, L. (2019a), "Modelling of crack propagation in rocks under SHPB impacts using a damage method", *Fatigue Fract. Eng. M.*, **42**(8), 1699-1710. https://doi.org/10.1111/ffe.13012.

Wang, M., Zhu, Z., Dong, Y. and Zhou, L. (2017), "Study of mixed-mode I/II fractures using single cleavage semicircle compression specimens under impacting loads", *Eng. Fract. Mech.*, **177**, 33-44. https://doi.org/10.1016/j.engfracmech.2017.03.042.

Wang, Q., Feng, F., Ni, M. and Gou, X. (2011), "Measurement of mode I and mode II rock dynamic fracture toughness with

cracked straight through flattened Brazilian disc impacted by split Hopkinson pressure bar", *Eng. Fract. Mech.*, **78**(12), 2455-2469. https://doi.org/10.1016/j.engfracmech.2011.06.004.

Wang, Q., Yang, J., Zhang, C., Zhou, Y., Li, L., Zhu, Z. and Wu, L. (2015), "Sequential determination of dynamic initiation and propagation toughness of rock using an experimental–numerical-analytical method", *Eng. Fract. Mech.*, **141**, 78-94. https://doi.org/10.1016/j.engfracmech.2015.04.025.

Wang, Q., Zhu, W., Xu, T., Niu, L. and Wei, J. (2016b), "Numerical simulation of rock creep behavior with a damage-based constitutive law", *Int. J. Geomech.*, **17**(1), 1-14. https://doi.org/10.1061/(ASCE)GM.1943-5622.0000707.

Wang, S.Y., Sloan, S.W., Sheng, D.C., Yang, S.Q. and Tang, C.A. (2014), "Numerical study of failure behaviour of pre-cracked rock specimens under conventional triaxial compression", *Int. J. Solids Struct.*, **51**(5), 1132-1148. https://doi.org/10.1016/j.ijsolstr.2013.12.012.

Wang, T., Song, Z., Yang, J., Wang, J. and Zhang, X. (2019b), "Experimental research on dynamic response of red sandstone soil under impact loads", *Geomech. Eng.*, **17**(4), 393-403. http://doi.org/10.12989/gae.2019.17.4.393.

Wang, Z., Shi, Y., Wang, J. and Zhang, Z. (2018), "Analysis of energy properties and failure modes of heat-treated granite in dynamic splitting test", *Geotech. Test. J.*, **41**(2), 235-246 .https://doi.org/10.1520/GTJ20170098.

Wei, Y., Ying, X., Wei, W. and Patrick, K. (2016), "Dependence of dynamic tensile strength of Longyou sandstone on heat-treatment temperature and loading rate", *Rock Mech. Rock Eng.*, **49**(10), 3899-3915.https://doi.org/10.1007/s00603-015-0895-7.

Wong, L.N.Y. and Li, H.Q. (2013), "Numerical study on coalescence of two pre-existing coplanar flaws in rock", *Int. J. Solids Struct.*, **50**(22-23), 3685-3706. https://doi.org/10.1016/j.ijsolstr.2013.07.010.

Wu, B., Yao, W. and Xia, K. (2016), "An experimental study of dynamic tensile failure of rocks subjected to hydrostatic confinement", *Rock Mech. Rock Eng.*, **49**(10), 3855-3864. https://doi.org/10.1007/s00603-016-0946-8.

Wu, F., Zhang, H., Zou, Q., Li, C., Chen, J. and Gao, R. (2020), "Viscoelastic-plastic damage creep model for salt rock based on fractional derivative theory", *Mech. Mater.*, **150**, 103600. https://doi.org/10.1016/j.mechmat.2020.103600.

Wu, Q., Chen, L., Shen, B., Dlamini, B. and Zhu, Y. (2019), "Experimental investigation on rockbolt performance under the tension load", *Rock Mech. Rock Eng.*, **52**(11), 4605-4618. https://doi.org/10.1007/s00603-019-01845-1.

Yang, S., Huang, Y. and Ranjith, P.G. (2018), "Failure mechanical and acoustic behavior of brine saturated-sandstone containing two pre-existing flaws under different confining pressures", *Eng. Fract. Mech.*, **193**, 108-121 .https://doi.org/10.1016/j.engfracmech.2018.02.021.

Yang, W., Yu, C. and Kobayashi, A.S. (1991), "SEM quantification of transgranular vs intergranular fracture", *J. Am. Ceram. Soc.*, **74**(2), 290-295. https://doi.org/10.1111/j.1151-2916.1991.tb06877.x.

Yi, L., Feng, D., Xu, N., Tao, Z. and Peng, F. (2018), "Experimental and numerical investigation on the tensile fatigue properties of rocks using the cyclic flattened Brazilian disc method", *Soil Dyn. Earthq. Eng.*, **105**, 68-82. https://doi.org/10.1016/j.soildyn.2017.11.025.

Yin, T., Li, X., Cao, W. and Xia, K. (2015), "Effects of thermal treatment on tensile strength of laurentian granite using brazilian test", *Rock Mech. Rock Eng.*, **48**(6), 2213-2223. https://doi.org/10.1007/s00603-015-0712-3.

Yuan, R. and Shen, B. (2017), "Numerical modelling of the contact condition of a Brazilian disk test and its influence on the tensile strength of rock", *Int. J. Rock Mech. Min. Sci.*, **93**, 54-65. https://doi.org/10.1016/j.ijrmms.2017.01.010.

Zhang, Q.B. and Zhao, J. (2013), "Determination of mechanical properties and full-field strain measurements of rock material under dynamic loads", *Int. J. Rock Mech. Min. Sci.*, **60**, 423-439. https://doi.org/10.1016/j.ijrmms.2013.01.005.

Zhang, Q.B. and Zhao, J. (2014), "Quasi-static and dynamic fracture behaviour of rock materials: Phenomena and mechanisms", *Int. J. Fracture.* **189**(1), 1-32. https://doi.org/10.1007/s10704-014-9959-z.

Zhang, Z., Xie, H., Zhang, R., Zhang, Z., Gao, M., Jia, Z. and Xie, J. (2018), "Damage and energy evolution characteristics of coal at different depths", *Rock Mech. Rock Eng.*, **52**(5), 1-13. https://doi.org/10.1007/s00603-018-1555-5.

Zhao, J. and Li, H. (2000), "Experimental determination of dynamic tensile properties of a granite", *Int. J. Rock Mech. Min. Sci.*, **37**(5), 861-866. https://doi.org/10.1016/S1365-1609(00)00015-0.

Zhou, L., Zhu, Z., Liu, B. and Fan, Y. (2018a), "The effect of radial cracks on tunnel stability", *Geomech. Eng.*, **15**(2), 721-728. https://doi.org/10.12989/gae.2018.15.2.721.

Zhou, L., Zhu, Z., Qiu, H., Zhang, X. and Lang, L. (2018b), "Study of the effect of loading rates on crack propagation velocity and rock fracture toughness using cracked tunnel specimens", *Int. J. Rock Mech. Min. Sci.*, **112**, 25-34. https://doi.org/10.1016/j.ijrmms.2018.10.011.

Zhou, Y.X., Xia, K., Li, X.B., Li, H.B., Ma, G.W., Zhao, J., Zhou, Z.L. and Dai, F. (2011), *Suggested Methods for Determining the Dynamic Strength Parameters and Mode-I Fracture Toughness of Rock Materials*, in *The ISRM Suggested Methods for Rock Characterization, Testing and Monitoring: 2007-2014*, Springer, Cham, Switzerland, 35-44.

Zhu, W.C., Niu, L.L., Li, S.H. and Xu, Z.H. (2015), "Brazilian test of rock under intermediate strain rate: Pendulum hammer-driven shpb test and numerical simulation", *Rock Mech. Rock Eng.*, **48**(5), 1867-1881. https://doi.org/10.1007/s00603-014-0677-7.

GC